

Testing the Non-circularity of the Spacetime around Sagittarius A* with Orbiting Pulsars

Yohsuke Takamori,^{1,*} Atsushi Naruko,² Yusuke Sakurai,³ Keitaro

Takahashi,^{4,5,6} Daisuke Yamauchi,⁷ and Chul-Moon Yoo³

¹ *National Institute of Technology (KOSEN),*

Wakayama College, Gobo, Wakayama 644-0023, Japan

² *Center for Gravitational Physics, Yukawa Institute for Theoretical Physics,*

Kyoto University, Kyoto 606-8502, Japan

³ *Division of Particle and Astrophysical Science,*

Graduate School of Science, Nagoya University, Nagoya 464-8602, Japan

⁴ *Kumamoto University, Graduate School of Science and Technology, Kumamoto, 860-8555, Japan*

⁵ *International Research Organization for Advanced Science and Technology,*

Kumamoto University, Kumamoto 860-8555, Japan

⁶ *National Astronomical Observatory of Japan,*

2-21-1 Osawa, Mitaka, Tokyo 181-8588, Japan

⁷ *Faculty of Engineering, Kanagawa University,*

Kanagawa-ku, Yokohama-shi, Kanagawa, 221-8686, Japan

A disformal Kerr black hole solution is a rotating black hole solution in a modified gravity theory which breaks the circular condition of spacetime differently from the case of the Kerr spacetime. In this paper, assuming that Sagittarius A* (Sgr A*) is a disformal Kerr black hole, we examine the potential to test the spacetime geometry with a hypothetical pulsar whose orbital elements are similar to those of the S2/S02 star. By numerically solving the equations of motion for the pulsar and photons emitted from it, we calculate the apparent position of the pulsar and the time of arrival (TOA) of the emitted pulse signals. Our analysis shows that the magnitude of the difference in the TOAs reaches the order of 10 ms if the deviation from the Kerr spacetime is significant. The time difference is mainly caused by the non-circularity of the spacetime at the 1.5 post-Newtonian order. The accuracy of the TOA measurement by a future radio telescope named the Square Kilometer Array (SKA) is between about 0.1 ms and 10 ms for a normal pulsar. Thus, we expect that the SKA can distinguish the disformal Kerr black hole from the Kerr black hole through the non-circularity of the spacetime around Sgr A*.

I. INTRODUCTION

The existence of black holes in our universe is a general prediction of general relativity, and the black holes are crucial in many aspects of cosmology and astrophysics. Astrophysical black holes can be classified by their mass, which is distributed in the wide range from about $1M_{\odot}$ to 10^9M_{\odot} . In general relativity, assuming vacuum environment, we can represent every black hole as the Kerr black hole thanks to the uniqueness theorem [1]. In the 2010s, a number of exciting observational discoveries about the black holes have been made. In 2015, the first detection of gravitational waves from a binary black hole has been achieved by the advanced Laser Interferometer Gravitational-Wave Observatory (aLIGO) and the Virgo [2]. Then, in 2018, the general relativistic effects in the dynamics of the star orbiting Sagittarius A* (Sgr A*) have been detected by the Very Large Telescope (VLT), the Keck telescope, and the Subaru telescope [3, 4]. Moreover, in 2019, the first image of the supermassive black hole in M87 has been successfully obtained by the Event Horizon Telescope (EHT) [5]. Those observational results are consistent with the Kerr black hole within their observational uncertainties.

One obviously attractive subject in observational research of black hole physics is the detection of the correction in gravitational theory beyond general relativity. Once obtaining a black hole solution in a modified gravity theory, it can be used as an alternative to the Kerr black hole. Deviation from the Kerr black hole implies modifications of the gravitational theory, and therefore we can test the validity of general relativity through the test of the Kerr black hole. Recently, a deformed Kerr black hole solution has been constructed in the context of the Degenerate Higher Order Scalar-Tensor (DHOST) theory (see the recent reviews of the DHOST theory [6, 7]), which is called the disformal Kerr black hole [8, 9]. The disformal Kerr black hole breaks the circular condition of spacetime, and the non-circularity of the disformal Kerr is characterized by a constant parameter D called the disformal parameter. When $D = 0$, the disformal Kerr metric reduces to the Kerr metric, and therefore the non-vanishing value of the disformal parameter D can be treated as a possible signal of the correction in the gravitational theory beyond general relativity. In Ref. [10], the authors have applied the disformal Kerr black hole to GRO J1655-40 and analyzed its observational data. As a result, they obtained the disformal parameter as $D = -0.010^{+0.011}_{-0.012}$ for GRO J1655-40. Moreover, the post-Newtonian (PN) motion of stars orbiting the disformal Kerr black hole has been analyzed with the osculating orbit method [11], and it is found that the secular

*Electronic address: takamori@wakayama-nct.ac.jp

evolution appears at 2PN order in generic D . They also pointed out that the secular evolution becomes significant when $D \sim -1$, and the secular shift due to the disformal parameter becomes comparable to the pericenter shift due to the Schwarzschild potential. In 2018, S2/S0-2 (hereafter S2) that is an orbiting star around Sgr A* passed through its pericenter, and it has been found that the pericenter shift is consistent with general relativity [12]. This observation of S2 would not allow the disformal Kerr black hole with $D \sim -1$ to represent Sgr A*.

This paper analyzes hypothetical pulsars orbiting Sgr A* assuming that Sgr A* can be well described by the disformal Kerr black hole with $D > -1$. Orbiting pulsars are suitable probes to study the spacetime around compact objects thanks to their accurate pulse period [13–16]. In the Galactic center region, orbiting stars within 0.02 pc have been discovered (see the review [17]). Some of them are young and massive, and they can leave a neutron star at the end of life. Some of the neutron stars would be observed as a normal pulsar, and not only main sequence stars but also pulsars could be orbiting Sgr A* [18, 19]. Although no normal pulsars have been detected within inner parsec yet [20–24], a magnetar whose distance from Sgr A* is ~ 0.1 pc was discovered [25–27]. In 2021, construction of a new facility named the Square Kilometer Array (SKA) has begun, which will be the largest radio telescope in the world. The SKA would detect about 14,000 normal pulsars [28], and some of them would be orbiting Sgr A*. In Ref. [29], the dynamics of a hypothetical pulsar on the S2-like orbit has been investigated with Sgr A* being the Kerr black hole. They have concluded that the spin of the central black hole is detectable by continuous monitoring of the hypothetical pulsar with the SKA. In this paper, we conduct a similar analysis by using the disformal Kerr black hole solution. Investigating a hypothetical orbiting pulsar with the orbital elements similar to S2, we find that the deviation from the Kerr in the arrival time of the pulse mainly comes from the non-circularity of the disformal Kerr at the 1.5PN order. Moreover, we discuss the detectability of the disformal parameter D by observations of the hypothetical pulsar with the SKA.

This paper is organized as follows. In Sec. II, we introduce the disformal Kerr solution. In Sec. III, we show our method to test the non-circularity of the spacetime around Sgr A* with hypothetical orbiting pulsars. The observables are the pulsar's position on the sky and the arrival time of the pulse. Those are determined by the motion of the pulsar and emitted photons, and the motion contains the effects of the non-circularity of the spacetime. We numerically solve the equations of motion with the Hamiltonian formalism and demonstrate the effects of the disformal parameter. In Sec. IV, we show results obtained by our simulation and discuss the detectability of D with the SKA. Finally, we summarize our work in the last section. Throughout this paper, we

set $c = G = 1$ where c and G are the speed of light and the gravitational constant, respectively.

II. DISFORMAL KERR SOLUTION

We summarize a derivation of the disformal Kerr solution [8, 9] and its properties. Let us consider the action of a scalar field with its higher derivatives:

$$S = \int d^4x \sqrt{-g} \left[P(X, \phi) + Q(X, \phi) \square \phi + F(X, \phi) R + \sum_{i=1}^5 A_i(X, \phi) L_i \right], \quad (1)$$

where P , Q , F , and A_i are functions depending on the scalar field ϕ and its kinetic term $X = \nabla_\mu \phi \nabla^\mu \phi$. ∇_μ is the covariant derivative associated with the metric $g_{\mu\nu}$, and R is the four-dimensional Ricci scalar. L_i are given by

$$\begin{aligned} L_1 &= \phi_{\mu\nu} \phi^{\mu\nu}, \quad L_2 = (\square \phi)^2, \quad L_3 = \phi^\mu \phi_{\mu\nu} \square \phi, \\ L_4 &= \phi^\mu \phi_{\mu\nu} \phi^{\nu\rho} \phi_\rho, \quad L_5 = (\phi^\mu \phi_{\mu\nu} \phi^\nu)^2, \end{aligned} \quad (2)$$

where $\phi_\mu = \nabla_\mu \phi$ and $\phi_{\mu\nu} = \nabla_\nu \nabla_\mu \phi$. In the DHOST theory, F and A_i are not free functions, and satisfy the specific conditions which guarantee the absence of ghost instabilities associated with the higher derivatives [30, 31]. In this paper, we focus on a subclass of DHOST theories, called the type-I DHOST. It is known that a DHOST theory with a set of free functions can be mapped to a different DHOST theory with another set of functions through a conformal-disformal transformation. The transformed metric $\tilde{g}_{\mu\nu}$ is expressed in terms of the original metric $g_{\mu\nu}$ and the scalar field ϕ as

$$\tilde{g}_{\mu\nu} = \mathcal{A}(X, \phi) g_{\mu\nu} + \mathcal{B}(X, \phi) \partial_\mu \phi \partial_\nu \phi. \quad (3)$$

This fact enables us to construct a new solution in a DHOST theory from an existing solution in another specific DHOST theory by performing a metric transformation.

Recently, a rotating black hole solution in a (subclass of type-I) DHOST theory was found [32]. Notably, its geometry is described by the Kerr solution while the scalar field has a nontrivial profile, and therefore the solution is called the stealth Kerr solution. The metric of the Kerr spacetime with a mass M and a spin a is written in the Boyer-Lindquist coordinates, (t, φ, r, θ) , as

$$g_{\mu\nu}^{\text{Kerr}} dx^\mu dx^\nu = - \left(1 - \frac{2Mr}{\rho^2} \right) dt^2 - \frac{4Mar \sin^2 \theta}{\rho^2} dt d\varphi + \frac{A \sin^2 \theta}{\rho^2} d\varphi^2 + \frac{\rho^2}{\Delta} dr^2 + \rho^2 d\theta^2, \quad (4)$$

where

$$\Delta = r^2 - 2Mr + a^2, \quad (5)$$

$$\rho^2 = r^2 + a^2 \cos^2 \theta, \quad (6)$$

$$A = (r^2 + a^2)^2 - a^2 \Delta \sin^2 \theta, \quad (7)$$

The spin parameter is restricted in the range $0 \leq |a/M| \leq 1$ for a black hole spacetime. The scalar field solution with a nontrivial configuration is given by

$$\phi = q \left[t + \int \frac{\sqrt{2Mr(a^2 + r^2)}}{r^2 - 2Mr + a^2} dr \right], \quad (8)$$

where q is a positive constant.

Applying a disformal transformation to the stealth Kerr solution, a new solution can be generated as

$$\tilde{g}_{\mu\nu}^{\text{Kerr}} = g_{\mu\nu}^{\text{Kerr}} - \frac{D}{q^2} \partial_\mu \phi \partial_\nu \phi, \quad (9)$$

where D is a constant called the disformal parameter. The set of $(\tilde{g}_{\mu\nu}^{\text{Kerr}}, \phi)$ is also an exact solution in a subclass of DHOST theories. Introducing the new time coordinate by $t \rightarrow t/\sqrt{1+D}$ in Eq. (9), namely $\tilde{g}_{\mu\nu}^{\text{Kerr}}[t/\sqrt{1+D}, \varphi, r, \theta] = g_{\mu\nu}^{\text{dKerr}}[t, \varphi, r, \theta]$, the metric of the disformal Kerr solution reads

$$\begin{aligned} & g_{\mu\nu}^{\text{dKerr}} dx^\mu dx^\nu \\ &= - \left(1 - \frac{2\tilde{M}r}{\rho^2} \right) dt^2 - \frac{4\sqrt{1+D}\tilde{M}r \sin^2 \theta}{\rho^2} dt d\varphi + \frac{A \sin^2 \theta}{\rho^2} d\varphi^2 \\ &+ \frac{\rho^2 \Delta - 2\tilde{M}(1+D)Dr(a^2 + r^2)}{\Delta^2} dr^2 - 2D \frac{\sqrt{2\tilde{M}r(a^2 + r^2)}}{\Delta} dt dr + \rho^2 d\theta^2. \end{aligned} \quad (10)$$

Here we have introduced the rescaled mass $\tilde{M} = M/(1+D)$. Note that the disformal parameter D should satisfy the inequality $D > -1$ in order that the new time coordinate is not imaginary, $t \rightarrow t/\sqrt{1+D}$. From the metric (10), we see that the mass and spin measured by a distant observer are given by \tilde{M} and $\tilde{a} = \sqrt{1+D}a$ not by M and a .

The most significant difference between the Kerr and the disformal Kerr is whether the cross term g_{tr} exists. In general relativity, the Kerr spacetime satisfies the circular condition which roughly implies the absence of cross terms between (t, φ) and (r, θ) . For $D = 0$, the cross term g_{tr} becomes zero, and then the metric (10) gives the Kerr's one in the Boyer-Lindquist coordinates. In the static limit that $a = 0$, non-zero g_{tr} remains, but it can be removed by the following coordinate transformation [9]:

$$dt = dT - \frac{D\sqrt{2\tilde{M}r^3}}{\Delta \left(1 - \frac{2\tilde{M}}{r} \right)} dr. \quad (11)$$

Then, the metric is written by

$$ds^2 = - \left(1 - \frac{2\tilde{M}}{r} \right) dT^2 + \left(1 - \frac{2\tilde{M}}{r} \right)^{-1} dr^2 + r^2 d\theta^2 + r^2 \sin^2 \theta d\varphi^2. \quad (12)$$

This represents the Schwarzschild spacetime with the rescaled mass \tilde{M} . Hence, the non-circularity of the disformal Kerr spacetime appears with the spin parameter.

The condition that the disformal Kerr spacetime has the event horizon constrains the parameters a and D , as is discussed in Ref. [9]. In the case $D \geq 0$, the critical value a_c is obtained by

$$a_c = \frac{\tilde{M}}{\sqrt{1+4D}}. \quad (13)$$

The spin parameter a should be in the range $|a| \leq a_c$ for the disformal Kerr spacetime to represent a black hole spacetime. In the case $-1 < D < 0$, one can obtain a polynomial equation for a_c (see Appendix B in [9]). The polynomial equation gives a finite value of a_c in the range $-1 < D < 0$. Taking the limit $D \rightarrow -1$, we obtain the critical value as $a_c \sim 0.516\tilde{M}$. Recall that the spin of the disformal Kerr is not a but $\tilde{a} = \sqrt{1+D}a$. In terms of \tilde{a} , the critical value for $D \geq 0$ is expressed as

$$\tilde{a}_c = \tilde{M} \sqrt{\frac{1+D}{1+4D}}. \quad (14)$$

For $D = 0$, which is the Kerr case, we have $\tilde{a}_c = \tilde{M}$. Taking the limit $D \rightarrow \infty$, the maximum spin becomes $\tilde{M}/2$. In the range $-1 \leq D < 0$, \tilde{a}_c approaches zero in the limit $D \rightarrow -1$ because $a_c \sim 0.516\tilde{M}$. This paper focuses on the parameter range for which the event horizon exists.

III. METHOD TO TEST THE NON-CIRCULARITY OF THE SPACETIME AROUND SGR A* WITH ORBITING PULSARS

Assuming that Sgr A* is a disformal Kerr black hole, we examine the motion of hypothetical pulsars on the orbit like S2. We call a pulsar whose orbital elements are similar to those of S2 a S2-like pulsar hereafter following Ref. [29]. We also assume that the standard matter fields including the pulsar and photons are minimally coupled with the disformal metric $g_{\mu\nu}^{\text{dKerr}}$. The ratio of the mass of the pulsar to that of Sgr A* is about 10^{-6} . Thus, the pulsar can be regarded as a test particle and follows a geodesic motion in the disformal Kerr spacetime. In Table I, we summarize the following parameters: the mass of the black hole, the distance to the Galactic center, and the typical orbital parameters of a S2-like pulsar.

TABLE I: Summary of the parameters.

Parameter	Description	Value
$M_{\text{BH}} (10^6 M_{\odot})$	Black Hole Mass	4.0
R_0 (kpc)	Distance to the Galactic Center	8.0
e	Eccentricity	0.88
T (yr)	Orbital Period	16
I (deg)	Inclination	135
ω (deg)	Argument of Periapsis	65
Ω (deg)	Longitude of Ascending Node	225

A. Coordinate transformation

We will examine the motion of the S2-like pulsar orbiting the disformal Kerr black hole with various a and D . Unfortunately, the original metric (10) is unsuitable for our purpose. Hence, we introduce a convenient coordinate system for our analysis below.

When $a = 0$, the metric (10) fails to recover the usual Schwarzschild metric due to the term g_{tr} . Moreover, g_{rr} in the metric obviously diverges when $\Delta = 0$. This is the coordinate singularity of the metric. Solving the equation $\Delta = 0$, we obtain the solutions for r as a function of \tilde{M} and \tilde{a} as follows:

$$\tilde{r}_{d\pm} = (1 + D)\tilde{M} \pm \sqrt{(1 + D)^2\tilde{M}^2 - \frac{\tilde{a}^2}{1 + D}}. \quad (15)$$

The periapsis distance of the S2-like pulsar is about $3000M_{\text{BH}}$. When $D \sim 1500$, the pulsar meets \tilde{r}_{d+} sometime. Therefore, solving the equation of motion for the S2-like pulsar, we face divergence when it passes through \tilde{r}_{d+} . In Ref. [9], the authors have given the following coordinate transformation:

$$dt = dT - D \frac{\sqrt{2\tilde{M}r(r^2 + a^2)}}{\Delta \left(1 - \frac{2\tilde{M}}{r}\right)} dr. \quad (16)$$

With these new coordinates, the cross term g_{Tr} is given by

$$g_{Tr} = \frac{2D\tilde{M}a^2 \cos^2 \theta \sqrt{2\tilde{M}r(r^2 + a^2)}}{(r - 2\tilde{M})\rho^2 \Delta}. \quad (17)$$

The cross term g_{Tr} vanishes when $a = 0$, and the usual Schwarzschild metric comes back. However, the coordinate singularity where $\Delta = 0$ still remains in Eq. (17). Therefore, that coordinate transformation is unsuitable for our purpose.

We shall consider a new coordinate system that reproduces the usual Schwarzschild metric without the coordinate singularity at $\Delta = 0$. Let us perform the following coordinate transformations to the metric (10):

$$dt = d\tilde{t} - \frac{D\sqrt{2\tilde{M}r(r^2 + a^2)^3}}{\tilde{\Delta}\Delta} dr, \quad (18)$$

$$d\varphi = d\tilde{\varphi} - \frac{Da\sqrt{2\tilde{M}r(r^2 + a^2)}}{\sqrt{1 + D\tilde{\Delta}\Delta}} dr, \quad (19)$$

where $\tilde{\Delta} = r^2 - 2\tilde{M}r + a^2$. Then, we have the metric with the new coordinates, $(\tilde{t}, \tilde{\varphi}, r, \theta)$, as

$$\begin{aligned} \tilde{g}_{\mu\nu}^{\text{dKerr}} dx^\mu dx^\nu &= - \left(1 - \frac{2\tilde{M}r}{\rho^2}\right) d\tilde{t}^2 - \frac{4\sqrt{1 + D\tilde{M}r} a \sin^2 \theta}{\rho^2} d\tilde{t} d\tilde{\varphi} + \frac{A \sin^2 \theta}{\rho^2} d\tilde{\varphi}^2 \\ &+ \frac{\rho^2 \tilde{\Delta} + D(r^2 + a^2)(\tilde{\Delta} - a^2 \sin^2 \theta)}{(1 + D)\tilde{\Delta}^2} dr^2 - \frac{2Da\sqrt{2\tilde{M}r(r^2 + a^2)} \sin^2 \theta}{\sqrt{1 + D\tilde{\Delta}}} dr d\tilde{\varphi} + \rho^2 d\theta^2. \end{aligned} \quad (20)$$

In this way, we can remove the coordinate singularity at $\Delta = 0$. The cross term $g_{r\tilde{\varphi}}$ appears instead of g_{tr} in the metric. In the asymptotic region $r \gg \tilde{M}$, the metric (20) is approximated by

$$\tilde{g}_{\mu\nu}^{\text{dKerr}} dx^\mu dx^\nu \sim -d\tilde{t}^2 + r^2 \sin^2 \theta d\tilde{\varphi}^2 + dr^2 + r^2 d\theta^2. \quad (21)$$

Thus, the new coordinates represent the well-known polar coordinates in the Minkowski spacetime in the asymptotic region. Furthermore, the metric (20) recovers the usual Schwarzschild metric when $a = 0$, as expected.

We can also find that g_{rr} in the metric (20) diverges when $\tilde{\Delta} = 0$, and this is the coordinate singularity of the metric. However, unlike the coordinate singularity at $\Delta = 0$, as is shown below, the coordinate singularity at $\tilde{\Delta} = 0$ is well inside the orbital radius of the S2-like pulsar, and we ignore this singularity in this work. Solving the equation $\tilde{\Delta} = 0$, we obtain the solutions as a function of \tilde{M} and \tilde{a} as

$$\tilde{r}_\pm = \tilde{M} \pm \sqrt{\tilde{M}^2 - \frac{\tilde{a}^2}{1 + D}}. \quad (22)$$

In general, \tilde{r}_+ is greater than \tilde{r}_- and outside the event horizon. Moreover, we can see that $\tilde{r}_+ \sim 2\tilde{M}$ for a generic D . Because the orbital radius of the S2-like pulsar is always greater than \tilde{r}_+ , the pulsar will not meet \tilde{r}_+ . Thus, the metric (20) is suitable for our purpose, and we solve the equations of motion for the S2-like pulsar and emitted photons with this metric.

B. Numerical method

This subsection shows our numerical method to solve the equations of motion for the S2-like pulsar and emitted photons. It should be noted that we hereinafter suppress tildes in the metric as well as the coordinate for the sake of notational simplicity.

1. Hamiltonian formalism

This work uses the Hamiltonian formalism, which is convenient to deal with both the pulsar motion and a photon trajectory [33]. Letting p_μ denote the four-momentum of the pulsar or a photon, we have the Hamiltonian as follows:

$$H = \frac{1}{2}g_{\text{dKerr}}^{\mu\nu}p_\mu p_\nu = -\frac{\kappa}{2}, \quad (23)$$

where $g_{\text{dKerr}}^{\mu\nu}$ is the inverse of $g_{\mu\nu}^{\text{dKerr}}$, and κ is the constant given by $\kappa = 1$ for the pulsar or $\kappa = 0$ for a photon. From the metric (20), the components of $g_{\text{dKerr}}^{\mu\nu}$ are given by

$$g_{\text{dKerr}}^{tt} = -\frac{(r^2 + a^2)^2 - a^2\tilde{\Delta}\sin^2\theta}{\tilde{\Delta}\rho^2} + \frac{4Da^2\tilde{M}^2r^2(r^2 + a^2)\sin^2\theta}{\tilde{\Delta}^2\rho^4}, \quad (24)$$

$$g_{\text{dKerr}}^{tr} = -\frac{2Da^2\sqrt{2\tilde{M}^3r^3(r^2 + a^2)}\sin^2\theta}{\tilde{\Delta}\rho^4}, \quad (25)$$

$$g_{\text{dKerr}}^{t\varphi} = -\frac{2\sqrt{1+D}\tilde{M}r}{\tilde{\Delta}\rho^2} + \frac{4Da^3\tilde{M}^2r^2\sin^2\theta}{\sqrt{1+D}\tilde{\Delta}^2\rho^4}, \quad (26)$$

$$g_{\text{dKerr}}^{rr} = \frac{\tilde{\Delta}}{\rho^2} + \frac{2Da^2\tilde{M}r\sin^2\theta}{\rho^4}, \quad (27)$$

$$g_{\text{dKerr}}^{r\varphi} = \frac{aD\sqrt{2\tilde{M}r(r^2 + a^2)}(\tilde{\Delta} - a^2\sin^2\theta)}{\sqrt{1+D}\tilde{\Delta}\rho^4}, \quad (28)$$

$$g_{\text{dKerr}}^{\theta\theta} = \frac{1}{\rho^2}, \quad (29)$$

$$g_{\text{dKerr}}^{\varphi\varphi} = \frac{\tilde{\Delta} - a^2\sin^2\theta}{\tilde{\Delta}\rho^2\sin^2\theta} - \frac{2Da^2\tilde{M}r(\tilde{\Delta} - a^2\sin^2\theta)}{(1+D)\tilde{\Delta}^2\rho^4}. \quad (30)$$

When numerically solving the equation of motion for photons emitted from an orbiting star, the pseudo-polar coordinates, (φ, r, θ) , are unsuitable [33]. This is because the photon travels to a distant observer being $8\text{ kpc} \sim 10^{10}M_{\text{BH}}$ away from the black hole, and the changes of the angular coordinates (φ, θ) are extremely small near the distant observer. Therefore, we use Cartesian-like coordinates to solve Hamilton's equations for the photons. This work simply uses the pseudo-Cartesian coordinates, (x, y, z) , defined by

$$x = r\sin\theta\cos\varphi, \quad y = r\sin\theta\sin\varphi, \quad z = r\cos\theta. \quad (31)$$

The pseudo-Cartesian coordinates represent the natural Cartesian coordinates in the asymptotic region $r \gg \tilde{M}$. With the pseudo-Cartesian coordinates, the spatial components of the four-momentum p_μ can be expressed as follows:

$$p_r = \frac{xp_x + yp_y + zp_z}{\sqrt{x^2 + y^2 + z^2}}, \quad (32)$$

$$p_\theta = \frac{z(xp_x + yp_y) - (x^2 + y^2)p_z}{\sqrt{x^2 + y^2}}, \quad (33)$$

$$p_\varphi = xp_y - yp_x. \quad (34)$$

When solving Hamilton's equations for the S2-like pulsar, we also use the pseudo-Cartesian coordinates. Finally, Hamilton's equations with the pseudo-Cartesian coordinates are written by

$$\frac{dp_\mu}{d\lambda} = -\frac{\partial H}{\partial x^\mu}, \quad \frac{dx^\mu}{d\lambda} = \frac{\partial H}{\partial p_\mu}, \quad (35)$$

where $p_\mu = (p_t(\lambda), p_x(\lambda), p_y(\lambda), p_z(\lambda))$ and $x^\mu = (t(\lambda), x(\lambda), y(\lambda), z(\lambda))$ with λ being an affine parameter. To avoid confusion, we use p_μ for the pulsar and k_μ for an emitted photon hereafter. For the pulsar, the affine parameter λ can be regarded as its proper time, and we replace λ with τ . To sum up, for the S2-like pulsar, we express Hamilton's equations as

$$\frac{dp_\mu}{d\tau} = -\frac{\partial H}{\partial x^\mu}, \quad \frac{dx^\mu}{d\tau} = \frac{\partial H}{\partial p_\mu}, \quad (36)$$

with $H = -1/2$. For an emitted photon, we have

$$\frac{dk_\mu}{d\lambda} = -\frac{\partial H}{\partial x^\mu}, \quad \frac{dx^\mu}{d\lambda} = \frac{\partial H}{\partial k_\mu}, \quad (37)$$

with $H = 0$.

2. Post-Newtonian and post-Minkowskian approximations

The S2-like pulsar is orbiting well far from the central black hole. Moreover, we do not consider photon trajectories passing through the vicinity of the central black hole. The post-Newtonian and post-Minkowskian approximations are available in that case [33]. Although we can perform the same analysis with the exact expression of the Hamiltonian, the post-Newtonian and post-Minkowskian expansions are helpful to classify and understand the effects of the disformal parameter D . This study uses the approximated Hamiltonian up to 2PN order because the effects up to 2PN order, which include the effects of the black hole spin and quadrupole moment, would be detectable in the SKA era.

For the S2-like pulsar, we have the following relation:

$$v^2 \sim \frac{M_{\text{BH}}}{r}, \quad (38)$$

where v is the speed of the pulsar. Let ϵ be a small parameter satisfying $0 < \epsilon \ll 1$ and $v \sim \epsilon$. Then, we can easily find that $r/M_{\text{BH}} \sim 1/v^2 \sim \epsilon^{-2}$. The time-component of the four-momentum, p_t , is the order of unity because it gives the rest mass of the pulsar. The r -component p_r is the order of ϵ because $p_r \sim v$. Moreover, we find that $p_\theta/r \sim p_\varphi/r \sim \epsilon$ because $p_\theta/r \sim p_\varphi/r \sim v$. Then, we can re-scale the four-momentum of the pulsar and r by ϵ as follows:

$$p_t \rightarrow p_t, \quad p_r \rightarrow \epsilon p_r, \quad p_\theta \rightarrow \epsilon^{-1} p_\theta, \quad p_\varphi \rightarrow \epsilon^{-1} p_\varphi, \quad r \rightarrow \epsilon^{-2} r. \quad (39)$$

By substituting Eqs. (39) to (23), we expand the Hamiltonian with respect to ϵ up to 2PN order. The approximated Hamiltonian for the pulsar is given by

$$H \approx \frac{1}{2} [H_0^{0\text{PN}} + \epsilon^2 H_2^{0\text{PN}} + \epsilon^4 H_4^{1\text{PN}} + \epsilon^5 H_5^{1.5\text{PN}} + \epsilon^6 H_6^{2\text{PN}}], \quad (40)$$

where

$$H_0^{0\text{PN}} = -p_t^2, \quad (41)$$

$$H_2^{0\text{PN}} = -\frac{2\tilde{M}}{r} p_t^2 + p_r^2 + \frac{p_\theta^2}{r^2} + \frac{p_\varphi^2}{r^2 \sin^2 \theta}, \quad (42)$$

$$H_4^{1\text{PN}} = -\frac{4\tilde{M}^2}{r^2} p_t^2 - \frac{2\tilde{M}}{r} p_r^2, \quad (43)$$

$$H_5^{1.5\text{PN}} = -\frac{4\tilde{a}\tilde{M}}{r^3} p_t p_\varphi + \frac{2D\tilde{a}}{1+D} \sqrt{\frac{2\tilde{M}}{r^5}} p_r p_\varphi, \quad (44)$$

$$H_6^{2\text{PN}} = -\frac{8(1+D)\tilde{M}^3 - 2\tilde{a}^2\tilde{M} \cos^2 \theta}{(1+D)r^3} p_t^2 + \frac{\tilde{a}^2 \sin^2 \theta}{(1+D)r^2} p_r^2 - \frac{\tilde{a}^2 \cos^2 \theta}{(1+D)r^4} p_\theta^2 - \frac{\tilde{a}^2}{(1+D)r^4 \sin^2 \theta} p_\varphi^2, \quad (45)$$

with $\tilde{a} = \sqrt{1+Da}$. The post-Newtonian order was shown with the superscripts. $H_0^{0\text{PN}}$ represents the rest mass of the S2-like pulsar, and $H_2^{0\text{PN}}$ produces the Kepler motion. $H_4^{1\text{PN}}$ is the weak-field Schwarzschild term that gives the pericenter shift. $H_5^{1.5\text{PN}}$ gives the frame-dragging effect due to the spin of the black hole. Then, the highest order term $H_6^{2\text{PN}}$ includes the quadrupole moment effects of the black hole proportional to \tilde{a}^2 . We find that the leading correction due to the disformal parameter D appears in $H_5^{1.5\text{PN}}$, and it gives the additional frame-dragging effect.

We can also expand the Hamiltonian for an emitted photon with a small parameter ϵ . This is called the post-Minkowskian expansion. We can assume that $r/M_{\text{BH}} \sim \epsilon^{-2}$ as was in the case of the S2-like pulsar, but, for the four-momentum of the photon, the order is different from the pulsar.

Because the photon travels with the speed of light, the four-momentum of the photon satisfies the relation $k_t \sim k_r \sim k_\theta/r \sim k_\varphi/r \sim 1$. Thus, we re-scale k_μ and r as follows:

$$k_t \rightarrow k_t, \quad k_r \rightarrow k_r, \quad k_\theta \rightarrow \epsilon^{-2} k_\theta, \quad k_\varphi \rightarrow \epsilon^{-2} k_\varphi, \quad r \rightarrow \epsilon^{-2} r. \quad (46)$$

By substituting Eq. (46) to Eq. (23), the Hamiltonian for the photon can be expanded up to the order of ϵ^6 which corresponds to 2PN order:

$$H \approx \frac{1}{2} [H_0^{0\text{PM}} + \epsilon^2 H_2^{1\text{PM}} + \epsilon^3 H_3^{1.5\text{PM}} + \epsilon^4 H_4^{2\text{PM}} + \epsilon^6 H_6^{3\text{PM}}], \quad (47)$$

where

$$H_0^{0\text{PM}} = -k_t^2 + k_r^2 + \frac{k_\theta^2}{r^2} + \frac{k_\varphi^2}{r^2 \sin^2 \theta}, \quad (48)$$

$$H_2^{1\text{PM}} = -\frac{2\tilde{M}}{r} k_t^2 - \frac{2\tilde{M}}{r} k_r^2, \quad (49)$$

$$H_3^{1.5\text{PM}} = \frac{2D\tilde{a}}{1+D} \sqrt{\frac{2\tilde{M}}{r^5}} k_r k_\varphi, \quad (50)$$

$$H_4^{2\text{PM}} = -\frac{4\tilde{M}^2}{r^2} k_t^2 + \frac{\tilde{a}^2 \sin^2 \theta}{(1+D)r^2} k_r^2 - \frac{\tilde{a}^2 \cos^2 \theta}{(1+D)r^4} k_\theta^2 - \frac{\tilde{a}^2}{(1+D)r^4 \sin^2 \theta} k_\varphi^2 - \frac{4\tilde{a}\tilde{M}}{r^3} k_t k_\varphi, \quad (51)$$

$$H_6^{3\text{PM}} = -\frac{8(1+D)\tilde{M}^3 - 2\tilde{a}^2\tilde{M} \cos^2 \theta}{(1+D)r^3} k_t^2 + \frac{2\tilde{a}^2\tilde{M}(\cos^2 \theta + D \sin^2 \theta)}{(1+D)r^3} k_r^2 - \frac{2(1+2D)\tilde{a}^2\tilde{M}}{(1+D)^2 r^5} k_\varphi^2 - \frac{8\tilde{a}\tilde{M}^2}{r^4} k_t k_\varphi. \quad (52)$$

The superscripts showed the post-Minkowskian (PM) order. $H_0^{0\text{PM}}$ produces a light-ray in the flat spacetime. $H_2^{1\text{PM}}$ represents the lens effect due to the weak-field Schwarzschild potential. The higher-order terms, $H_4^{2\text{PM}}$ and $H_6^{3\text{PM}}$, include the effects of the black hole spin and quadrupole moment. For the photon motion, unlike the pulsar motion, the leading correction due to the disformal parameter D appears in $H_3^{1.5\text{PM}}$. Since there is no corresponding term in the case of the Kerr solution, this correction causes the stronger light bending in the φ -direction than in the usual Kerr correction.

3. Motion of the S2-like pulsar and the initial conditions

This work uses the Kepler motion to determine the initial conditions for the motion of the S2-like pulsar. Let the coordinates of the orbital plane be (X, Y) . The Kepler motion with the eccentricity e can be expressed by

$$X(u) = s(\cos u - e), \quad (53)$$

$$Y(u) = s\sqrt{1-e^2} \sin u, \quad (54)$$

where u is the eccentric anomaly and s is the semi-major axis. The origin of u is at the pericenter. In the Kepler motion, the derivative of u with respect to the coordinate time t is given by

$$\frac{du}{dt} = \sqrt{\frac{M_{\text{BH}}}{s^3}} \frac{1}{1 - e \cos u}. \quad (55)$$

Thus, the components of the velocity on the orbital plane is given by

$$V_X(u) = \frac{dX}{dt} = -\sqrt{\frac{M_{\text{BH}}}{s}} \frac{\sin u}{1 - e \cos u}, \quad (56)$$

$$V_Y(u) = \frac{dY}{dt} = \sqrt{\frac{M_{\text{BH}}}{s}} \frac{\sqrt{1 - e^2} \cos u}{1 - e \cos u}. \quad (57)$$

For the sake of simplicity, we fix a distant observer at $(x, y, z) = (0, 0, -R_0)$ in the pseudo-Cartesian coordinates. Then, the position and the velocity of the Kepler motion in the pseudo-Cartesian coordinates are given by

$$x(u) = (X \cos \omega - Y \sin \omega) \cos \Omega - (Y \cos \omega + X \sin \omega) \sin \Omega \cos I, \quad (58)$$

$$y(u) = (Y \cos \omega + X \sin \omega) \cos \Omega \cos I + (X \cos \omega - Y \sin \omega) \sin \Omega, \quad (59)$$

$$z(u) = (Y \cos \omega + X \sin \omega) \sin I, \quad (60)$$

and

$$v_x(u) = (V_X \cos \omega - V_Y \sin \omega) \cos \Omega - (V_Y \cos \omega + V_X \sin \omega) \sin \Omega \cos I, \quad (61)$$

$$v_y(u) = (V_Y \cos \omega + V_X \sin \omega) \cos \Omega \cos I + (V_X \cos \omega - V_Y \sin \omega) \sin \Omega, \quad (62)$$

$$v_z(u) = (V_Y \cos \omega + V_X \sin \omega) \sin I, \quad (63)$$

where I , ω , and Ω are the inclination, the argument of periapsis, and the longitude of ascending node, respectively. We choose the apocenter at $u = \pi$ as the initial position. Finally, the initial conditions for the motion of the S2-like pulsar are given by

$$x_0 = x(\pi), \quad y_0 = y(\pi), \quad z_0 = z(\pi), \quad (64)$$

$$p_{x0} = v_x(\pi), \quad p_{y0} = v_y(\pi), \quad p_{z0} = v_z(\pi). \quad (65)$$

Given x_0 , y_0 , z_0 , p_{x0} , p_{y0} , and p_{z0} , the Hamiltonian constraint that $H = -1/2$ becomes a quadratic equation for p_t that is a conserved quantity of motion. We solve the quadratic equation and choose the negative root. To numerically solve Hamilton's equations for the pulsar, we use the Dromand-Prince method that is the explicit fifth(forth)-order Runge-Kutta method implemented in *Mathematica*. We should check if the Hamiltonian constraint is satisfied in the numerical integration. The integration continues until the pulsar comes back to the apocenter again. The relative integration errors are $\leq \mathcal{O}(10^{-15})$ during the calculation.

4. Photon trajectories from the S2-like pulsar to the distant observer

This study requires photon trajectories from the S2-like pulsar to the distant observer, but we do not know the initial k_μ that gives the trajectory a priori. Our procedure to find the initial k_μ is shown here.

We assume that a photon emitted at $\lambda = 0$ hits the distant observer at $\lambda = 1$. Giving the initial conditions for the photon motion, the position of the photon at $\lambda = 1$ is obtained by solving Hamilton's equations for the photon. Then, we can express the coordinate deviations between the photon position x_i^{hit} at $\lambda = 1$ and the observer position x_i^{obs} as functions of the initial three momentum of the photon k_j^{em} as follows [33]:

$$f_i(k_j^{\text{em}}(\tau); \tau) = x_i^{\text{hit}}(k_j^{\text{em}}(\tau)) - x_i^{\text{obs}}, \quad (66)$$

where the τ dependence of k_j^{em} has been explicitly shown with the argument, namely, $k_j^{\text{em}}(\tau) = k_j|_{\lambda=0}$ is the three-momentum of an emitted photon from the pulsar at $(x(\tau), y(\tau), z(\tau))$. This work uses the Newton-Raphson method to find k_j^{em} that satisfies $f_i(k_j^{\text{em}}) = 0$. In practice, we give the criterion for k_j^{em} as

$$\sqrt{(x^{\text{hit}} - x^{\text{obs}})^2 + (y^{\text{hit}} - y^{\text{obs}})^2 + (z^{\text{hit}} - z^{\text{obs}})^2} < 10^{-7} M_{\text{BH}}. \quad (67)$$

Because the radius of a neutron star would be $\sim 10^{-5} M_{\text{BH}}$, the above criterion is sufficient for our purpose. Moreover, we set the distant observer at $(x^{\text{obs}}, y^{\text{obs}}, z^{\text{obs}}) = (0, 0, -10^8 M_{\text{BH}})$ rather than $(0, 0, -R_0)$, where $R_0 \sim 10^{10} M_{\text{BH}}$, to search k_j^{em} efficiently as in Refs. [29, 34]. The changes of the observables due to the replacement of the observer position are smaller than the observational uncertainties in the SKA. To obtain x_i^{hit} , we numerically solve Hamilton's equations for the photon with the Dromand-Prince method. k_t^{em} is determined by the Hamiltonian constraint that $H = 0$ with the initial conditions of the photon. k_t^{em} is the conserved quantity of motion, and then we check whether the Hamiltonian constraint is satisfied during the calculation. We see that $|H|/(k_t^{\text{em}})^2 \leq \mathcal{O}(10^{-14})$ in the integration.

C. Apparent position and the time of arrival

We show our formalism to express the position of the S2-like pulsar on the sky and the arrival time of the pulse here. This study focuses on the gravitational effect due to the disformal Kerr black hole. We ignore other environmental effects such as the effect of the interstellar medium.

1. Apparent position on the sky

The pulsar's position is given on the sky plane (α, β) , where α is the right accession and β is the declination angle. We can relate the angular position to the apparent position in the pseudo-Cartesian coordinates, $(x_{\text{ap}}, y_{\text{ap}})$, as

$$\alpha = -\frac{y_{\text{ap}}}{R_0}, \quad \beta = \frac{x_{\text{ap}}}{R_0}. \quad (68)$$

The apparent position $(x_{\text{ap}}, y_{\text{ap}})$ can be determined by the four-momentum of an emitted photon arriving at the distant observer. Let the four-momentum of the photon at $\lambda = 1$ be k_{μ}^{hit} , that is, $k_{\mu}^{\text{hit}} = k_{\mu}|_{\lambda=1}$. From the view of the observer, the photon is coming from the direction of the vector k_{μ}^{hit} . Thus, solving the equation of motion for the photon with $-k_{\mu}^{\text{hit}}$ in the Minkowski spacetime, we can obtain the apparent position of the pulsar in the pseudo-Cartesian coordinates as follows:

$$x_{\text{ap}} = -k_x^{\text{hit}}, \quad y_{\text{ap}} = -k_y^{\text{hit}}. \quad (69)$$

Usually, the proper motion of Sgr A* on the sky is added to Eq. (68) (e.g., see [29] for pulsar studies). Because the proper motion of Sgr A* is canceled out when we see the difference between the disformal Kerr and Kerr, this study uses Eq. (68) with Eq. (69) for the angular position of the S2-like pulsar.

2. Time of arrival

We calculate the time of arrival (TOA) of the pulse without environment effects between the central black hole and the distant observer for the sake of simplicity. Then the TOA is purely determined by the redshift of emitted photons, Z , which can be written by

$$Z = \frac{p^{\mu} k_{\mu}^{\text{em}}}{U_{\text{obs}}^{\mu} k_{\mu}^{\text{hit}}} - 1, \quad (70)$$

where U_{obs}^{μ} is the four-velocity of the distant observer given by $U_{\text{obs}}^{\mu} = (1, 0, 0, 0)$ in the pseudo-Cartesian coordinates. We easily see that $U_{\text{obs}}^{\mu} k_{\mu}^{\text{hit}} = k_t^{\text{hit}} = k_t^{\text{em}}$ because the time component of k_{μ} is the conserved quantity of motion. Thus, Eq. (70) can be expressed as

$$Z = \frac{p^{\mu} k_{\mu}^{\text{em}}}{k_t^{\text{em}}} - 1. \quad (71)$$

p_{μ} and k_{μ}^{em} are given at each proper time of the S2-like pulsar. Then, we can calculate the TOA by the following integral with respect to the proper time [29]:

$$t_{\text{TOA}}(\tau) = \int_0^{\tau} (Z(\tilde{\tau}) + 1) d\tilde{\tau}. \quad (72)$$

It would be helpful to show the approximated redshift in the post-Newtonian and post-Minkowskian approximations. The redshift can be expanded up to 2PN+3PM order (the order of ϵ^6) as follows:

$$\begin{aligned}
Z + 1 \approx & -p_t + \epsilon \left(\frac{p_r k_r^{\text{em}}}{k_t^{\text{em}}} + \frac{1}{r^2} \frac{p_\theta k_\theta^{\text{em}}}{k_t^{\text{em}}} + \frac{1}{r^2 \sin^2 \theta} \frac{p_\varphi k_\varphi^{\text{em}}}{k_t^{\text{em}}} \right) - \epsilon^2 \frac{2\tilde{M}}{r} p_t - \epsilon^3 \frac{2\tilde{M}}{r} \frac{p_r k_r^{\text{em}}}{k_t^{\text{em}}} \\
& + \epsilon^4 \left(-\frac{4\tilde{M}^2}{r^2} p_t - \frac{2\tilde{a}\tilde{M}}{r^3} \frac{p_t k_\varphi^{\text{em}}}{k_t^{\text{em}}} + \frac{D\tilde{a}}{1+D} \sqrt{\frac{2\tilde{M}}{r^5}} \frac{p_r k_\varphi^{\text{em}}}{k_t^{\text{em}}} + \frac{D\tilde{a}}{1+D} \sqrt{\frac{2\tilde{M}}{r^5}} \frac{p_\varphi k_r^{\text{em}}}{k_t^{\text{em}}} \right) \\
& + \epsilon^5 \left(-\frac{2\tilde{a}\tilde{M}}{r^3} p_\varphi + \frac{\tilde{a}^2 \sin^2 \theta}{(1+D)r^2} \frac{p_r k_r^{\text{em}}}{k_t^{\text{em}}} - \frac{\tilde{a}^2 \cos^2 \theta}{(1+D)r^4} \frac{p_\theta k_\theta^{\text{em}}}{k_t^{\text{em}}} - \frac{\tilde{a}^2}{(1+D)r^4 \sin^2 \theta} \frac{p_\varphi k_\varphi^{\text{em}}}{k_t^{\text{em}}} \right) \\
& + \epsilon^6 \left(-\frac{8(1+D)\tilde{M}^3 - 2\tilde{a}^2\tilde{M} \cos^2 \theta}{(1+D)r^3} p_t - \frac{4\tilde{a}\tilde{M}^2}{r^4} \frac{p_t k_\varphi^{\text{em}}}{k_t^{\text{em}}} \right). \tag{73}
\end{aligned}$$

We find that the leading correction of the TOA due to the disformal parameter D appears in the 1.5PN+2PM order (the order of ϵ^4).

D. Test case: differences between the Kerr and the Schwarzschild

Before we investigate the disformal Kerr black hole with various sets of (\tilde{a}, D) , let us see the case of the Kerr black hole as a test. We calculate the apparent position and the TOA for the S2-like pulsar in the cases of the extremal Kerr $(\tilde{a}_*, D) = (1, 0)$ and the Schwarzschild $(\tilde{a}_*, D) = (0, 0)$, where $\tilde{a}_* = \tilde{a}/\tilde{M}$. In Fig. 1, we show the apparent position and the time evolution of the redshift measured in the proper time τ in the case of $(\tilde{a}_*, D) = (1, 0)$. Then, we compare the results of those cases and show the differences in Fig. 2. Here we express the difference between the values in the cases of the extremal Kerr and the Schwarzschild by δ , namely, for example, $\delta\alpha = \alpha|_{\tilde{a}_*=1} - \alpha|_{\tilde{a}_*=0}$. The spin-induced difference in the apparent position is on the order of $1 \mu\text{as}$, and, for the redshift, the maximum of the difference is on the order of $10^{-2} \text{ km} \cdot \text{s}^{-1}$. These values are consistent with the previous studies [34]. The spin-induced difference in the TOA is shown in Fig. 3. This is consistent with the result given in Ref. [29]. The expected astrometric accuracy of the SKA is $10 \mu\text{as}$. For the TOA, the accuracy is from 0.1 ms to 10 ms , which varies with the observed frequencies. In Fig. 2(a), the spin-induced effects in the apparent position is smaller than the astrometric accuracy $10 \mu\text{as}$ within the time interval taken for Fig. 2(a). However, the difference secularly increases as the S2-like pulsar orbits Sgr A*. Then the difference in the apparent position becomes detectable within a few periods ($< 50 \text{ yr}$). For the TOA, from Fig. 3, the spin-induced effect is obviously far larger than its accuracy, and it is detectable with the SKA [29].

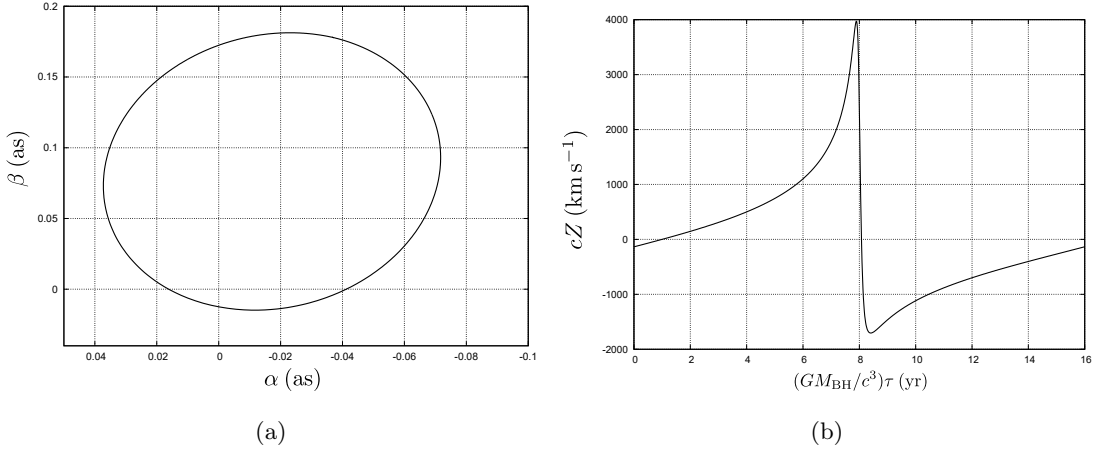


FIG. 1: Apparent position of the S2-like pulsar (a) and time evolution of the redshift of photons from the pulsar (b). The time used in the panel (b) is the proper time of the S2-like pulsar.

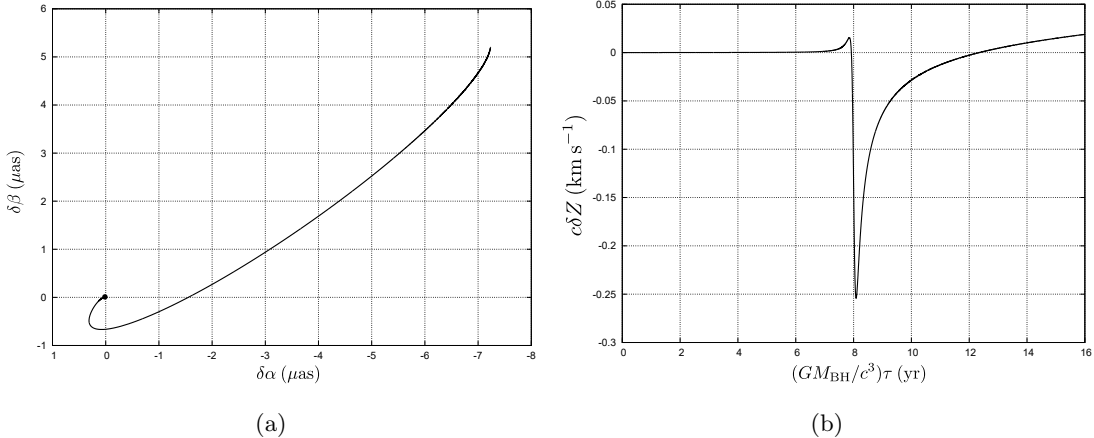


FIG. 2: Differences between the Kerr and the Schwarzschild. The difference in the apparent position, $(\delta\alpha, \delta\beta)$, is in the panel (a). The filled circle represents the difference at $\tau = 0$, and the difference does not come back to the initial position due to the apocenter shift. The difference in the redshift, $c\delta Z$, is in the panel (b). As in the panel (a), we can see the secular effect due to the apocenter shift.

IV. EFFECTS OF THE DISFORMAL PARAMETER D AND ITS DETECTABILITY WITH THE SKA

We investigate the disformal Kerr black hole with various sets of (\tilde{a}_*, D) and show the effects of the disformal parameter D . Moreover, we discuss the detectability of the disformal parameter D with the SKA. The parameters used in our simulations are summarized in Table II. First, we examine the motion of the S2-like pulsar with some sets of (\tilde{a}_*, D) where the spin parameter \tilde{a}_* is set

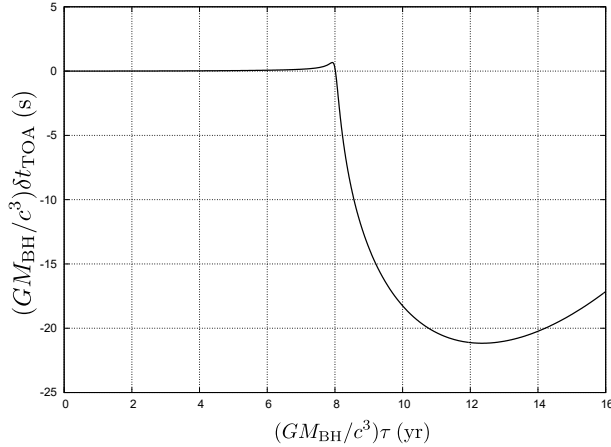


FIG. 3: Spin-induced effect in t_{TOA} . δt_{TOA} represents the difference in TOA between the Kerr and the Schwarzschild.

to be 0.1, 0.5, and 0.7. The parameter range of D in which the disformal Kerr spacetime describes a black hole spacetime depends on the value of \tilde{a}_* . Let $D_+(\tilde{a}_*)$ and $D_-(\tilde{a}_*)$ denote the upper and lower values of D for a fixed value of \tilde{a}_* , respectively. For $\tilde{a}_* \leq 0.5$, there is no upper value for D , that is, we can take $D_+ \rightarrow \infty$. On the other hand, the lower value is in $-1 < D_-(\tilde{a}_*) < 0$. From the paper [9], we can obtain $D_-(\tilde{a}_*)$ as $D_-(0.1) \sim -0.96$, and $D_-(0.5) \sim -0.41$. In the case $\tilde{a}_* > 0.5$, both the upper and lower values are obtained. For $\tilde{a}_* = 0.7$, we obtain $D_-(0.7) \sim -0.17$ and $D_+(0.7) \sim 0.53$. We pick up some D within $D_-(\tilde{a}_*) < D < D_+(\tilde{a}_*)$ for each \tilde{a}_* .

Next, we change the inclination angle to $I = 180^\circ$ (face-on) and $I = 95^\circ$ (nearly edge-on) for the S2-like pulsar in Case II and III, respectively, and consider three values of the eccentricity: $e = 0$, 0.4, and 0.88. Note that when using the inclination angle that $I = 90^\circ$ (edge-on), pulsars may almost overlap behind the central black hole on the line-of-sight. Then we have to seriously take the strong gravitational lensing effect due to the black hole into account. To avoid this situation, this study uses the value that $I = 95^\circ$.

A. Results

For each case in Table II, the apparent position and the TOA are obtained. Moreover, we perform our simulations without the disformal parameter D and then compare the results with and without D . The difference is denoted by δ as in the previous section, namely, $\delta\alpha = \alpha|_{(\tilde{a}_*=0.1,D=1)} - \alpha|_{(\tilde{a}_*=0.1,D=0)}$, for example. We demonstrate the results for Case I, II, and III in the following subsections, respectively.

TABLE II: Summary of the parameter sets for Case I (S2-like), Case II (face-on) and III (nearly edge-on).

Case	$\tilde{a}_* = \tilde{a}/M_{\text{BH}}$	D	$(e, T, I, \omega, \Omega)$
I(a)	0.1	-0.9, -0.8, -0.6, 1, 10, and 1000	(0.88, 16, 135, 65, 225)
I(b)	0.5	-0.4, -0.2, 0.5, 1, 10, and 1000	(0.88, 16, 135, 65, 225)
I(c)	0.7	-0.1, 0.1, 0.2, and 0.5	(0.88, 16, 135, 65, 225)
II(a)	0.5	1	(0, 16, 180, 65, 225)
II(b)	0.5	1	(0.4, 16, 180, 65, 225)
II(c)	0.5	1	(0.88, 16, 180, 65, 225)
III(a)	0.5	1	(0, 16, 95, 65, 225)
III(b)	0.5	1	(0.4, 16, 95, 65, 225)
III(c)	0.5	1	(0.88, 16, 95, 65, 225)

1. Effects of the disformal parameter D at 1.5PN, 2PN and higher PN order terms

The effect of the disformal parameter D appears from 1.5PN order in the Hamiltonian for the S2-like pulsar. To see the significance of the terms at each order, we calculate the apparent position and the TOA taking the terms up to 1.5PN+2PM order (the order of ϵ^4), 2PN+3PM order (the order of ϵ^6), and full order (without the PN and PM expansions), and compare them with each other. We choose the case $D = 1$ in Case I(b) and calculate $\delta\alpha$, $\delta\beta$, and δt_{TOA} in each order. The differences in each order are shown in Fig. 4. From the figures, we find that the deviation from the Kerr is mostly determined by the 1.5PN+2PM approximation. It means that the non-circularity of the spacetime at the 1.5PN order, which also gives the 1.5PM order, mainly produces the deviation. From Fig. 4(a), we can see the apocenter shift due to the disformal parameter D appears in the case of the 2PN+3PM approximation. Although the effect of the disformal parameter D appears at the 1.5PN order in the pulsar motion, a significant secular apocenter shift appears at the 2PN order. It is consistent with the previous study [11] where they have shown that the secular shift of the motion appears at 2PN order in generic D . We can also see the effect of the apocenter shift in δt_{TOA} from Fig. 4(b). The TOA is given by the integration of the redshift, and therefore the secular shift due to the 2PN order becomes significant in the second half of the orbit. Since we do not find any significant corrections from the higher-order terms in the post-Newtonian and post-Minkowskian approximations in Fig. 4, hereafter, we show all the results with the equations up to 2PN+3PM order.

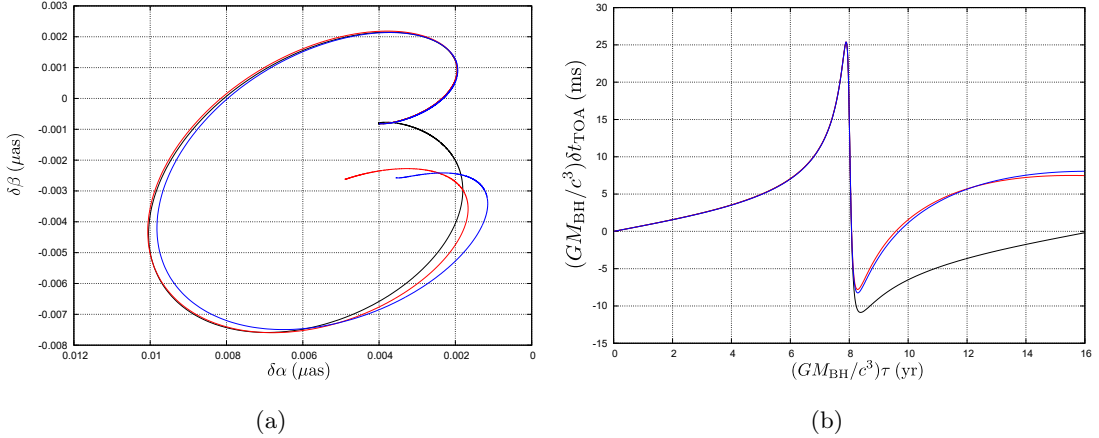


FIG. 4: Differences in the apparent position (a) and the TOA (b) between the cases that $(\tilde{a}_*, D) = (0.5, 1)$ and $(0.5, 0)$. The black and red solid lines represent the results from the 1.5PN+2PM and 2PN+3PM approximations, respectively. The blue solid lines come from the full order equations. We see that a significant apocenter shift appears in the 2PN+3PM approximation from both the panels. We also find that the higher-order terms in the full order equations does not add any significant corrections to the results in the 2PN+3PM approximation. In the panel (a), $(\delta\alpha, \delta\beta)$ at $\tau = 0$ is off the origin. Although the initial positions of the S2-like pulsar are the same in both the disformal Kerr and Kerr cases, the apparent positions are different from each other in general because of the difference in the photon trajectory.

2. Case I (S2-like: inclination angle $I = 135^\circ$)

We have examined three different spin parameters: $\tilde{a}_* = 0.1, 0.5$, and 0.7 . The differences in the apparent position and the TOA are shown in Figs. 5, 6 and 7. From Figs. 5(a), 6(a) and 7(a), we find that $|\delta\alpha|$ and $|\delta\beta|$ are in the range from 10^{-3} to 10^{-2} μas . From Figs. 5(b), 6(b) and 7(b), we find that $|\delta t_{\text{TOA}}|$ reaches the 10 ms order. We also find that, although the disformal Kerr metric reduces to the Schwarzschild metric in the static limit with a finite value of D , since the possible range of D is wider for smaller \tilde{a}_* , the effect of the disformal parameter D can be more significant for a smaller value of \tilde{a}_* .

3. Case II (face-on: inclination angle $I = 180^\circ$)

The results are shown in Fig. 8. We find that $|\delta\alpha|$ and $|\delta\beta|$ are the order of 10^{-2} μas . The value of the apocenter shift is larger as the eccentricity increased. The maximum values of δt_{TOA} is about 1 ms at around the half of the period as is shown in Fig. 8(b).

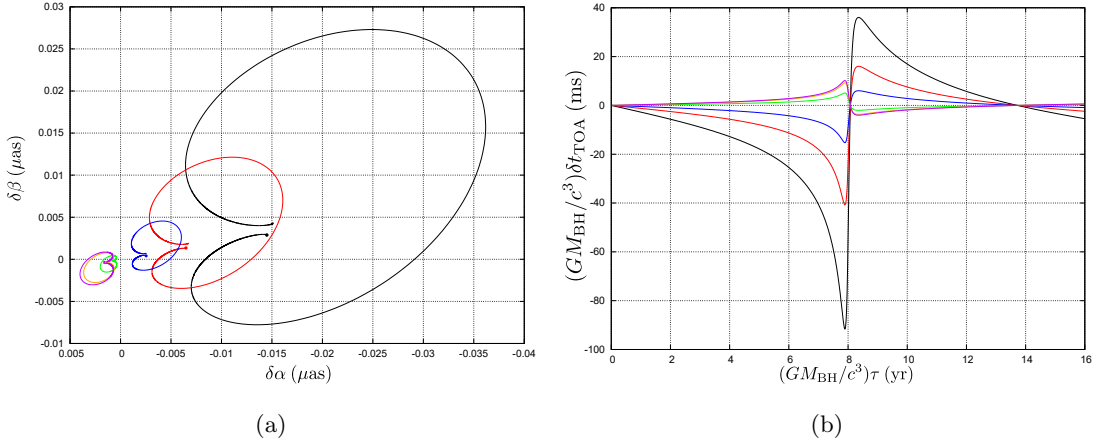


FIG. 5: Differences in the apparent position (a) and the TOA (b) in the case $\tilde{a}_* = 0.1$. We show $(\delta\alpha, \delta\beta)$ and δt_{TOA} in the cases that $D = -0.9$ (black), -0.4 (red), -0.6 (blue), 1 (green), 10 (orange), and 1000 (magenta). The filled circles in the panel (a) represent $(\delta\alpha, \delta\beta)$ at $\tau = 0$.

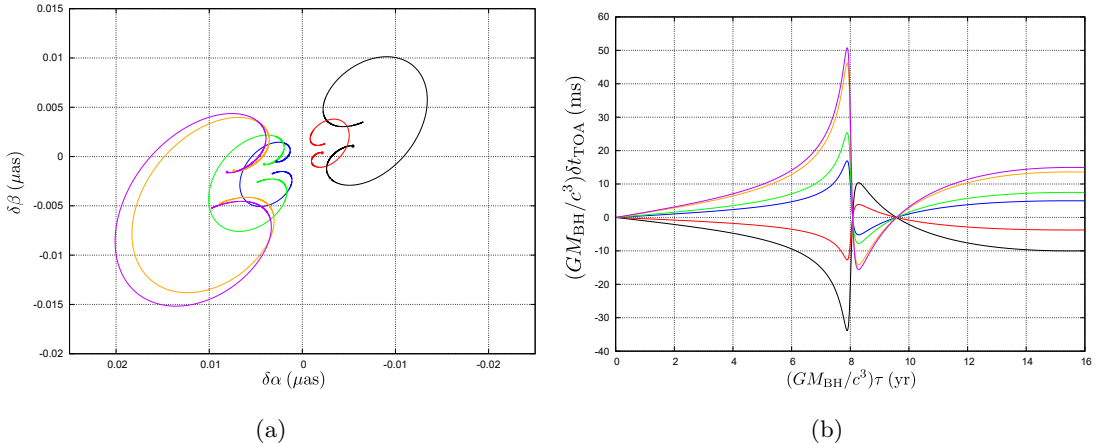


FIG. 6: Differences in the apparent position (a) and the TOA (b) in the case $\tilde{a}_* = 0.5$. The solid lines with colors represent the cases that $D = -0.4$ (black), -0.2 (red), 0.5 (blue), 1 (green), 10 (orange), and 1000 (magenta).

4. Case III (nearly edge-on: inclination angle $I = 95^\circ$)

The results are shown in Fig. 9. We find that $|\delta\alpha|$ and $|\delta\beta|$ are at the order of $10^{-3} \mu\text{as}$, which is smaller than those of the face-on case. The maximum value of $|\delta t_{TOA}|$ can be 10 ms order, which is greater than that of the face-on case. We also observe the significant apocenter shift for the case $e = 0.88$.

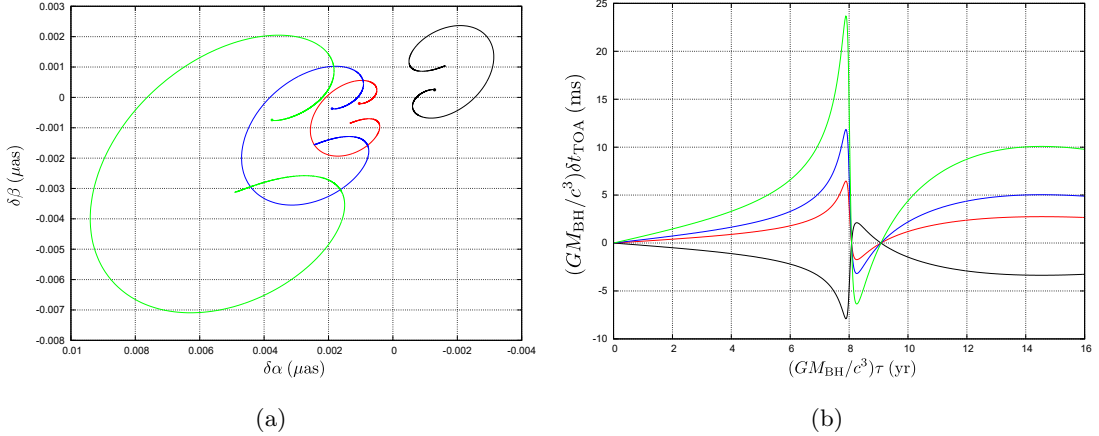


FIG. 7: Differences in the apparent position (a) and the TOA (b) in the case $\tilde{a}_* = 0.7$. The solid lines with colors are the cases that $D = -0.1$ (black), 0.1 (red), 0.2 (blue), and 0.5 (green).

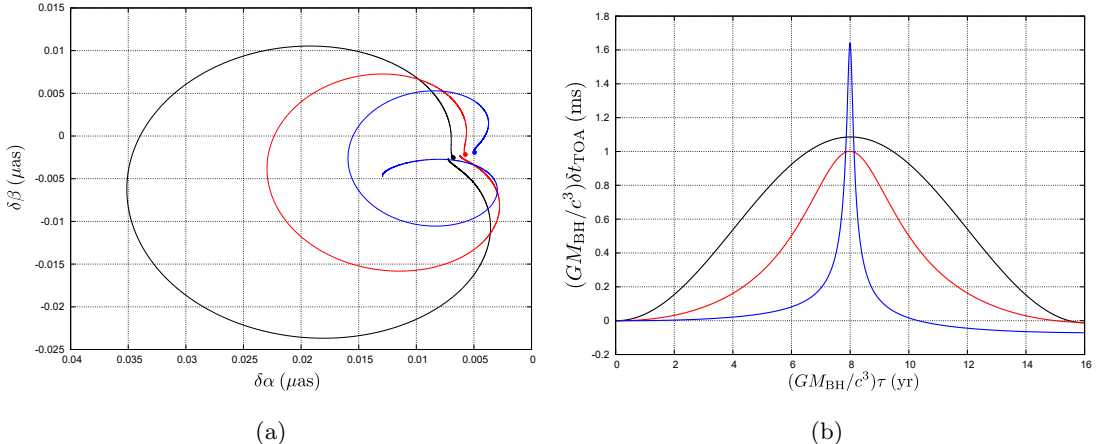


FIG. 8: Differences in the apparent position (a) and the TOA (b) in the face-on case $I = 180^\circ$. The black, red, and blue solid lines show the cases that $e = 0, 0.4$, and 0.88 , respectively.

B. Detectability of the disformal parameter D with the SKA

We have calculated the apparent positions and the TOAs for each of the S2-like, face-on and nearly edge-on pulsars in Case I, II, and III, respectively. Here, we briefly discuss whether we can distinguish the disformal Kerr from the Kerr by observing such pulsars by the SKA.

First, let us focus on the apparent position. From Figs. 5(a), 6(a) and 7(a), $|\delta\alpha|$ and $|\delta\beta|$ are in the range from 10^{-3} to 10^{-2} μas per orbit. In Case II and III, the differences in the apparent position are almost the same in Case I. The SKA could detect the apparent position of the pulsar with $10 \mu\text{as}$ accuracy. Thus, we conclude that it is hard to detect the sign of the disformal Kerr

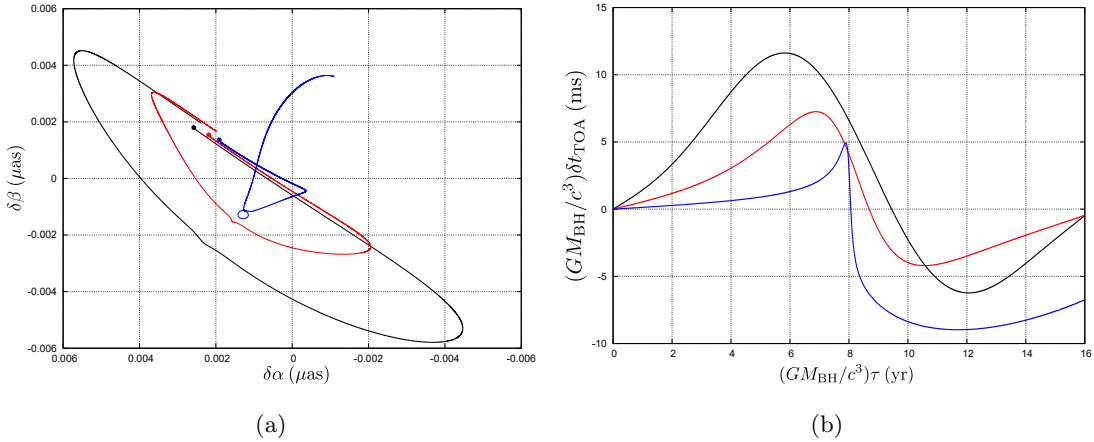


FIG. 9: Differences in the apparent position (a) and the TOA (b) in the nearly edge-on case $I = 95^\circ$. The black, red, and blue solid lines show the cases that $e = 0, 0.4$, and 0.88 , respectively.

black hole from the astrometric observation of pulsars on the orbit like S2 by the SKA.

Next, let us see the differences in the TOAs. In Case I, from Figs. 5(b), 6(b) and 7(b), the maximum values of $|\delta t_{\text{TOA}}|$ reach 10 ms order when $|D| \gtrsim 0.1$. The accuracy of the TOA with the SKA is within 0.1 to 10 ms for a normal pulsar, and therefore the differences in the TOA are sufficiently large for the detection. In Case II and III, we can find the typical magnitude of δt_{TOA} from Figs. 8(b) and 9(b). Focusing on Case II (nearly edge-on), the maximum values of $|\delta t_{\text{TOA}}|$ is at the order of 10 ms. Since the value of δt_{TOA} is almost linearly dependent on the parameter D , we may conclude that the disformal parameter $|D| > 0.1$ would be detectable with the observation of pulsars on the orbit like S2 by the SKA.

V. SUMMARY AND DISCUSSION

Detecting the possible deviations from the Kerr spacetime is an attractive subject to investigate a theory of gravity beyond general relativity. Recently, an exact solution called the disformal Kerr black hole solution has been constructed in a subclass of DHOST theories, and the deviation from the Kerr solution is characterized by a constant parameter D . In this paper, we have examined observational aspects of a hypothetical S2-like pulsar orbiting Sgr A* by assuming that Sgr A* is a disformal Kerr black hole. We numerically solved the equations of motion the S2-like pulsar and photons emitted from it with the Hamiltonian formalism. Then, we have shown how the disformal parameter D affects the motion of the S2-like pulsar and the time of arrival of emitted photons. Moreover, we discussed the detectability of the disformal parameter D by a future radio telescope

named the Square Kilometer Array (SKA).

First, we investigated a hypothetical S2-like pulsar orbiting a disformal Kerr black hole with the spin parameters $\tilde{a}_* = 0.1, 0.5$, and 0.7 . We found that the difference of the apparent position of the pulsar between the disformal Kerr and Kerr cases is about $10^{-2} \mu\text{as}$ per orbit at most. It is smaller than the expected uncertainty of the SKA, that is $10 \mu\text{as}$. As for the emitted pulses, we estimated that the difference of the times of arrival between two cases can be at the order of 10 ms for $|D| \gtrsim 0.1$. This difference in the arrival time of the pulses is sufficiently large for the detection with the SKA. Thus the SKA can probe the non-circularity of the spacetime around Sgr A* at 1.5PN order since the difference is mainly caused by the non-circularity of the spacetime at the order of 1.5PN . Note that the allowed parameter range of the disformal parameter D is restricted depending on the spin parameter. For the case of a rapidly rotating black hole, the allowed range of D is small compared to the case of a slowly rotating black hole. In the case of the spin parameter with $\tilde{a}_* \gtrsim 0.88$, the allowed disformal parameter is smaller than 0.1 . We could not distinguish the disformal Kerr black hole with $\tilde{a}_* \gtrsim 0.88$ from the Kerr spacetime by the SKA. Although we do not know the spin parameter for Sgr A* exactly, it is estimated to be in the range $|\tilde{a}_*| \leq 0.5$ [35, 36]. Sgr A* can be a good candidate for the testing site of the disformal Kerr black hole since the allowed range of D is large for a slowly rotating black hole. Aside from a specific theory of modified gravity, since the non-circularity implies the deviation from the Kerr spacetime, one can perform an effective test of general relativity through the non-circularity of the spacetime around Sgr A* with the SKA.

Finally we make a comment on the constraint obtained by gravitational wave observations. It should be noted that, from the nearly simultaneous detection of the gravitational-wave and gamma-ray signals from a neutron-star merger event GW170817 [37], the difference between the speed of gravitational waves and that of light is tightly constrained [38]. In the DHOST theory, the speed of gravitational waves differs from the speed of light in general and the theory that we have used in this paper is not exceptional. Hence, the theory, at least a part of the theory, will not be viable on cosmological scales due to the above constraint. Nevertheless, we hope that the black hole at the Galactic center can provide a complementary test of modified gravity on different scales beside tests on cosmological scales.

Acknowledgements

This work was supported by JSPS KAKENHI Grant Numbers JP19H00695, JP19H01900 (Y. T.), 20H05852 (A.N.), JP19H01891 (A.N. and D.Y.), 17H01110, 20H00180, 21H01130, 21H04467 (K.T.), 17K14304 (D.Y.), JP19H01895, JP20H05850 and JP20H05853 (C.Y.), Bilateral Joint Research Projects of JSPS (K.T.), and the ISM Cooperative Research Program [2020-ISMCRP-2017] (K.T.).

- [1] D. C. Robinson, Phys. Rev. Lett. **34**, 905 (1975).
- [2] B. P. Abbott *et al.* [LIGO Scientific and Virgo], Phys. Rev. Lett. **116**, 061102 (2016).
- [3] R. Abuter *et al.* [GRAVITY collabo.], Astron. Astrophys. **615**, L15 (2018).
- [4] T. Do *et al.*, Science **365**, 664 (2019).
- [5] K. Akiyama *et al.* [EHT collabo.], Astrophys. J. Lett. **875**, L1 (2019).
- [6] T. Kobayashi, Rep. Prog. Phys. **82**, 086901 (2019).
- [7] D. Langlois, Int. J. Mod. Phys. D **28**, 1942006-3287 (2019).
- [8] J. B. Achour, H. Liu, H. Motohashi, S. Mukohyama, and K. Noui, J. Cosmo. Astropart. Phys. **11**, 001 (2020).
- [9] T. Anson, E. Babichev, C. Charmousis, and M. Hassaine, J. High Energy Phys. **2021**, 18 (2021).
- [10] S. Chen, Z. Wang, and J. Jing, arXiv:2103.11788 (2021).
- [11] T. Anson, E. Babichev, and C. Charmousis, Phys. Rev. D **103**, 124035 (2021).
- [12] R. Abuter *et al.* [GRAVITY collabo.], Astron. Astrophys. **636**, L5 (2020).
- [13] N. Wex and S. M. Kopeikin, Astrophys. J. **514**, 388 (1999).
- [14] M. Kramer *et al.*, Science **314**, 97 (2006).
- [15] K. Liu, N. Wex, M. Kramer, J. M. Cordes, T. J. W. Lazio, Astrophys. J. **747**, 1 (2012).
- [16] D. Psaltis, N. Wex, and M. Kramer, Astrophys. J. **818**, 121 (2016).
- [17] R. Genzel, F. Eisenhauer, and S. Gillessen, Rev. Mod. Phys. **82**, 3121 (2010).
- [18] E. Pfahl and A. Loeb, Astrophys. J. **615**, 253 (2004).
- [19] R. S. Wharton, S. Chatterjee, J. M. Cordes, J. S. Deneva, and T. J. W. Lazio, Astrophys. J. **753**, 108 (2012).
- [20] J. S. Deneva, J. M. Cordes, and T. J. W. Lazio, Astrophys. J. Lett. **702**, L177 (2009).
- [21] J. P. Macquart, N. Kanekar, D. A. Frail, and S. M. Ransom, Astrophys. J. **715**, 939 (2010).
- [22] S. D. Bates *et al.*, Mon. Not. Roy. Astron. Soc. **411**, 1575 (2011).
- [23] P. Torne *et al.*, Astron. Astrophys. **650**, A95 (2021).
- [24] K. Liu *et al.*, Astrophys. J. **914**, 30 (2021).
- [25] K. Mori *et al.*, Astrophys. J. Lett. **770**, L23 (2013).

- [26] J. A. Kennea *et al.*, *Astrophys. J. Lett.* **770**, L24 (2013).
- [27] R. P. Eatough *et al.*, *Nature (London)* **501**, 391 (2013).
- [28] R. Smits, M. Kramer, B. Stappers, D. R. Lorimer, J. Cordes, A. Faulkner, *Astron. Astrophys.* **493**, 1161 (2009).
- [29] F. Zhang and P. Saha, *Astrophys. J.* **849**, 33 (2017).
- [30] D. Langlois and K. Noui, *J. Cosmo. Astropart. Phys.* **2016**, 034 (2016)
- [31] J. B. Achour, D. Langlois, and K. Noui, *Phys. Rev. D* **93**, 124005 (2016).
- [32] C. Charmousis, M. Crisostomi, R. Gregory, and N. Stergioulas, *Phys. Rev. D* **100**, 084020 (2019).
- [33] R. Angélil and P. Saha, *Astrophys. J.* **711**, 157 (2010).
- [34] F. Zhang, Y. Lu, and Q. Yu, *Astrophys. J.* **809**, 127 (2015).
- [35] Y. Kato, M. Miyoshi, R. Takahashi, H. Negoro, and R. Matsumoto, *Mon. Not. Roy. Astron. Soc.* **403**, L74 (2010).
- [36] G. Fragione and A. Loeb, *Astrophys. J. Lett.* **901**, L32 (2020).
- [37] B. P. Abbott *et al.* [LIGO Scientific and Virgo], *Phys. Rev. Lett.* **119**, 161101 (2017).
- [38] M. J. Ezquiaga and M. Zumalacárregui, *Front. Astron. Space Sci.* **5**, 44 (2018).